Proceedings of the INMM & ESARDA Joint Virtual Annual Meeting
August 23-26 & August 30-September 1, 2021

Feasibility of Fast Neutron Imaging of Spent Nuclear Fuel Dry Storage Casks

Z. Liu[a,*], M. Fang[a], A. Di Fulvio[a]

[a]*Department of Nuclear, Plasma, and Radiological Engineering,*
University of Illinois, Urbana-Champaign,
104 South Wright Street, Urbana, IL 61801, United States

Abstract

In recent years, the need to store spent nuclear fuel (SNF) using Dry casks has been increasing. However, the nondestructive assay of the SNF is a challenging task due to the thick sealed steel enclosure. In this paper we performed an imaging reconstruction study of the SNF canister based on a Monte Carlo simulation of a realistic dry storage cask system. We simulated the active interrogation of the SNF canister using 14.1 MeV neutrons from a D-T neutron generator and identified the back-scattered neutron signature which can be used in the image reconstruction process. We carried out the image reconstruction of the canister using a iterative linear inverse approach with the maximum number of iterations set to 10^6 and obtained well reconstructed images for the peripheral assembly missing scenarios. Then, we applied the pre-trained convolutional neural network (CNN) to the reconstructed images of the inner assembly missing scenarios from the iterative linear inverse approach. The output of the CNN shows that the image quality for the inner assembly missing scenarios can be further improved.

Keywords: Neutron tomography, Spent nuclear fuel, Dry cask storage, Nondestructive assay, Fast Iterative Shrinkage-Thresholding Algorithm, Convolutional neural network

1. Introduction

The storage of SNF assemblies is a crucial part of the fuel cycle. SNF assemblies are first put into water pools upon fuel removal from the core. Once the capacity of the water pools are reached, the SNF assemblies are transferred from at-reactor water pools to final storage sites which are always far away from the nuclear power plant. In recent years, there has been a raising in the need for transporting SNF assemblies to either away-from-reactor reprocessing plants or permanent storage sites [1]. Dry storage casks can be used as an interim storage during the transportation and also the final storage containers at final storage sites, thus the inspection of dry storage casks becomes very significant. Dry storage casks have thick side walls and sealed top covers, which are commonly made of steel or concrete. Thus dry storage casks can ensure the safe storage of SNF assemblies and also provide enough radiation shielding. However, this enclosure also makes verifying the condition of the inside SNF assemblies without reopening the sealed casks an open technical challenge.

Continuity of knowledge (CoK) is the commonly used safeguards measurement to ensure the safe storage of the SNF assemblies. CoK is a system of data or information regarding an item that is uninterrupted and authentic and provides the International Atomic Energy Agency (IAEA) with adequate insight to draw definitive conclusions that nuclear material is not being diverted from peaceful purposes [2]. CoK is typically ensured using seals and visual observation; however, reestablishment of inventory may be required after the loss of CoK. Once the CoK is lost, the correctness and completeness of the previous knowledge can not be valid. To reestablish the CoK, image reconstruction techniques for the spent fuel dry casks could be employed to reconstruct the missing information. The interruption of the CoK can then be addressed with the verified information of the SNF in the dry cask. Therefore, it is critical to develop a non-destructive method to re-assure the content and integrity of the dry storage casks.

Among the proposed non-destructive inspection methods, the most promising one seems to be the cosmic-ray muon tomography method [3] [4] [5]. However, it requires long inspection times of the order of more than one day and thus it is impractical to check the cask's integrity after a potential incident during transportation.

*Corresponding author. Tel.: 2179043453
Email address: zhihual2@illinois.edu (Z. Liu)

In this paper, we present a method based on 14.1 MeV neutron tomography. This method aims at identifying potential fuel diversion scenarios, where the fuel is removed from the canister. First, we studied the sensitivity of the inspection method to missing assemblies. We studied the signatures that showed the highest correlations with the missing SNF assembly. Then, we used the identified signatures to carry out the neutron tomography technique and obtain the reconstructed images of the canister.

2. Geant4 Model and Back-scattered Neutron Signature

We modeled a simplified design of a dry storage cask which consists of HI-STAR-100 cask, MPC-68 canister and basket, and GE-14 fuel assembly using Geant4 [6]. The realistic fuel system is very detailed and takes too long to perform the simulation. So we developed a simplified model with homogenized fuel assembly to shorten simulation run time while keeping a realistic fuel composition. In the simplified model, the fuel assembly contains a mixture of the same material compositions distributed throughout the whole assembly volume. While yielding similar results in terms of neutron scattering and transmitted distribution, the run-time of the simplified model is approximately eight times faster than the detailed model. Therefore, we decided to proceed with the simplified model. We chose to apply the QGSP_BERT_HP physics list to ensure high-precision neutron transport simulation at energies below 20 MeV. The source term was simulated as a pencil beam at first, with a mono-energetic energy of 14.1 MeV. It was placed at the mid-plane of the cask targeting at the side surface.

Since the canister and the fuel deployment are symmetric, we carried out the study on one-quarter of the canister first to investigate the sensitivity of the inspection method to missing assemblies. Fig. 1 shows the missing fuel assembly locations in simulated eight diversion scenarios named as Case1 to Case8 and we also simulated one full loaded canister (named as Case0). In each diversion scenario, one fuel assembly in the corresponding numbered location is removed from the canister. The neutron beam has a traveling direction as shown in the red arrow in Fig. 1. Neutrons coming out from the surface of the canister are recorded.

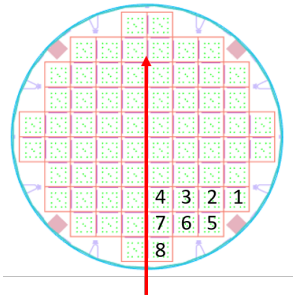

Figure 1: Canister geometry and assembly locations for the eight diversion scenarios.

We analyzed the angular distribution of the neutrons and found that the back-scattered neutrons are the most informative signature. We compared the the neutrons distribution of Case0 with the other eight diversion cases. Fig. 2 shows the relative difference between the fully loaded case and eight diversion scenarios along the canister surface. In Fig. 2, the x-axis represents the central angle of the canister with the neutron beam traveling direction passing through the central angle 0^o. Y-axis is calculated using the following equation: $\mathbf{y} = \frac{N_{Casei} - N_{Case0}}{N_{Case0}}$, where $\mathbf{i}$ is from 1 to 8 and N represents the back-scattered neutrons reaching the surface of the canister within the corresponding central angle range.

From Fig. 2, we can see that whenever there's fuel assembly missing, a corresponding change in the neutron counts is detected and these changes show a certain relationship with the location of the missing fuel assembly. For the purpose of image reconstruction, we select the angle $10^o - 30^o$ with respect to the neutron beam direction as the detection region for the back-scattered neutrons since the change of neutron counts shows a consistent drop in the diversion scenarios.

3. Computational Methods

Since CoK typically uses seals and visual observation, it is hard to reestablish it without reopening the sealed canister if CoK is lost. Hence, it is necessary to develop an imaging verification method for the inspection of the sealed canister independent of CoK. In our research, we consider the back-scattered signature and only the measurements at a few angles

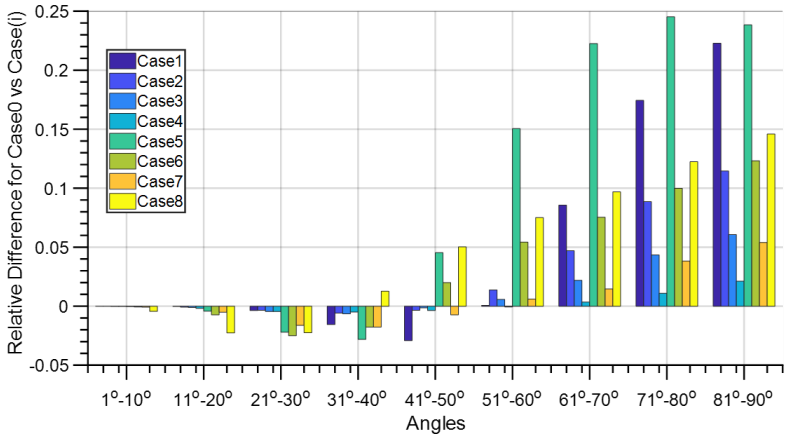

Figure 2: Neutron counts distribution difference between fully loaded case and the eight diversion cases within 90^o degree with respect to the neutron beam direction.

with respect to the interrogating neutron beam are informative, therefore the traditional filtered back projection (FBP) algorithm is not practical. The Fast Iterative Shrinkage-Thresholding Algorithm (FISTA) can be applied when we treat the imaging of the dry storage casks as a linear inverse problem. FISTA is an alternative method to FBP algorithm for sparse data in imaging reconstruction. It has been proved to successfully reconstruct a PWR spent fuel assembly reduced reconstruction artifacts with respect to FBP [7].

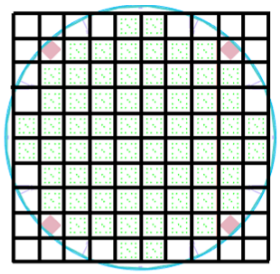

Figure 3: An example of the discretization of the region of interest ($\mathbf{N} = 10$).

First, we reconstructed the spent-fuel cask cross-sectional image acquired through neutron tomography. The tomographic inspection consisted oftwelve scans around the cask, in 30° intervals. We discretized the dry storage cask region into $N \times N$ pixels as shown in Fig. 3 (where $N = 10$ as an example) to reconstruct the cask image. Based on the linear model, the neutron signal emerging from the surface of the cask as the signal $\mathbf{y}$ can be calculated using the following equation (Equation 1):

$$\mathbf{y} = \mathbf{A}\mathbf{x} + \mathbf{n} \tag{1}$$

Where $\mathbf{A}$ is the system response matrix that can be calculated through simulation, $\mathbf{x}$ is signal response of each pixel to the incident neutron beam, and $\mathbf{n}$ is the random observation noise. By solving the inverse problem in Eq. 1 through FISTA as shown below, we can obtain the distribution of the fuel assemblies inside the dry storage cask.

FISTA with constant step size [8]:

Input: $\mathbf{A}$, $\mathbf{y}$, L: The Lipschitz constant of $\mathbf{A}$, λ (depending on noise level).

Procedure:

1. Set the initial values:
   $\mathbf{z}^{(1)} = 0$, $\mathbf{x}^{(0)} = 0$, $t_1 = 1$ and $k_{\max}$: *total number of iterations*.
2. When $1 \leq k \leq k_{\max}$ is satisfied, the algorithm will do an iteration until $k_{\max}$ is reached with the following steps:

$$x^{(k)} = z^{(k)} - \frac{1}{L} A^T (A z^{(k)} - \mathbf{y}) \tag{2}$$

$$x^{(k)} = \max(x^{(k)} - \frac{\lambda}{L}, 0) \tag{3}$$

$$t_{k+1} = \frac{1 + \sqrt{1 + 4t_k^2}}{2} \tag{4}$$

$$z^{(k+1)} = x^{(k)} + \frac{t_k - 1}{t_{k+1}}(x^{(k)} - x^{(k-1)}) \tag{5}$$

Output: $\hat{\mathbf{x}} = x^{(k)}$.

It will finally return the value $\hat{\mathbf{x}} = x^{(k)}$, i.e. the reconstructed image, when the set total number of iterations is reached.

The CNN can denoise the reconstructed images obtained by some commonly used image reconstruction algorithms. Thus, a reconstructed images can be obtained with improved quality without increasing the exposure of radiation. The application of a CNN to the images obtained through the iterative reconstruction algorithm FISTA improves the image quality of the inner assemblies [9].

Fig. 4 shows the architecture of the CNN model used in this study. We use high-quality reconstructed images as the ground truth and low-quality reconstructed images as the input to the network. After the model is trained, we can then use it to predict the location of missing fuel pins in the inner region of the canister.

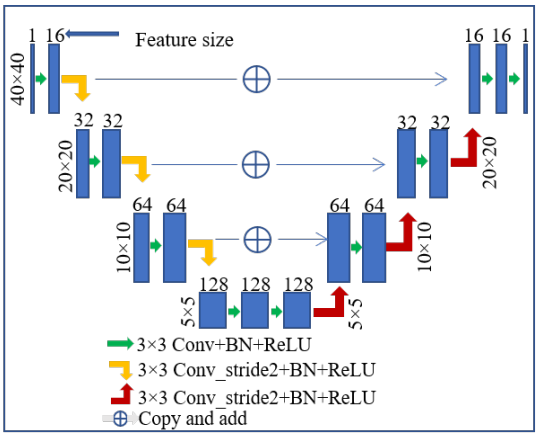

Figure 4: Schematic diagram of the CNN architecture.

4. Response Matrix and Interpolation

Fig. 5 shows the simulated system response matrix **A** as a function of number of pixels for the twelve scans, which is based on the discretization in Fig. 3 with **N**=10, for the detection angle $20^o - 30^o$. The unit of the color bar is neutron counts per source neutron.

We increased the resolution of the response matrix through cubic interpolation. The interpolated response is a 12×1600 matrix, as compared to the original 12×100. The interpolated response matrix was used in the image reconstruction algorithms.

5. Iterative Image Reconstruction

Fig. 6 shows the ground truth and the reconstructed image from FISTA algorithm when the maximum number of iterations is set to 10^6. The reconstructed images quality is affected by many factor such as maximum number of iterarions of the FISTA algorithm, measurement time which is related with the level of noise of the readout **y** and the location of the missing fuel pins. Hence, we need to define a metric that can be used to evaluate the quality of the reconstructed images. Here, we choose to calculate the signal-to-noise ratio between the reconstructed image and the ground truth to evaluate the reconstructed image qualities.

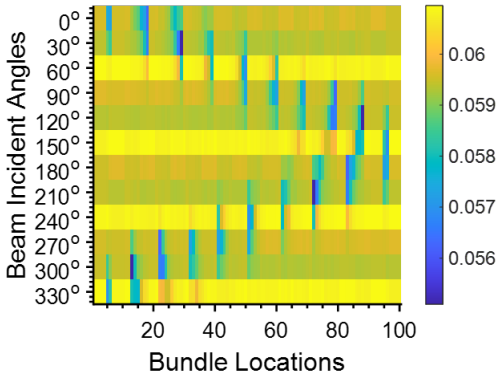

Figure 5: Simulated response matrix for back-scattered neutrons within detection angle $20^o - 30^o$ for discretization with $N = 10$.

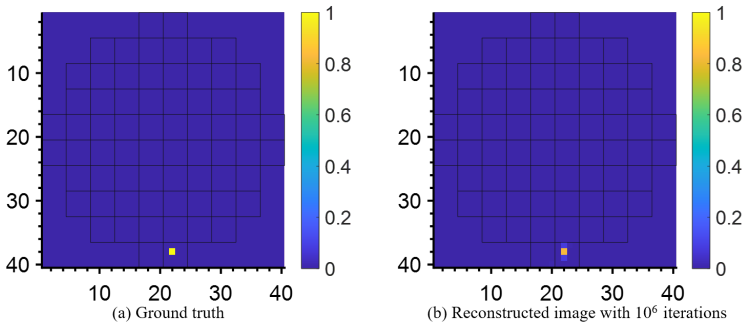

Figure 6: Ground truth and reconstructed image from FISTA algorithm with maximum iteration = 10^6 for peripheral assembly missing scenario.

The signal-to-noise ratio (SNR) used in this paper is defined as Eq. 6 [10].

$$\textbf{SNR} = 10 \times \log_{10} \frac{mean(f(x,y)^2)}{\textbf{MSE}} \tag{6}$$

where $\textbf{MSE} = \frac{1}{\textbf{MN}} \sum_{x=0}^{M-1} \sum_{y=0}^{N-1} [f(x,y) - \hat{f}(x,y)]^2$ is the mean square error between the reconstructed image $\hat{f}(x,y)$ and the ground truth $f(x,y)$.

We removed the fuel pins from the selected location as shown in Fig. 7 ground truth. Then, we applied the FISTA algorithm to the measured data and obtained reconstructed images with different number of iterations. Fig. 7 shows that the image quality improves with the number of iterations. However, the computation time will also increase dramatically and can be up to hours for a single image reconstruction.

Table 1 shows the SNR for maximum number of iterations larger than 10^6. We can see that the SNR does not significantly improve for a number of iterations higher than 10^6. Therefore, we set the maximum number of iterations for the FISTA algorithm at 10^6 which ensures a good image quality while maintaining a reasonable computation time. We also tested this setting of iterations on other assembly locations and it proved to be effective for other locations too. The results show that with iterations equal to 10^6, we can reconstruct the images where $\frac{1}{16}$ pins of one fuel assembly were removed.

Table 1: Relationship between SNR and iteration in assembly location [22,36] which is the same as Fig. 7.

Iterations	SNR
7×10^6	27.577
10^7	27.677
1.5×10^7	27.687
2×10^7	27.713

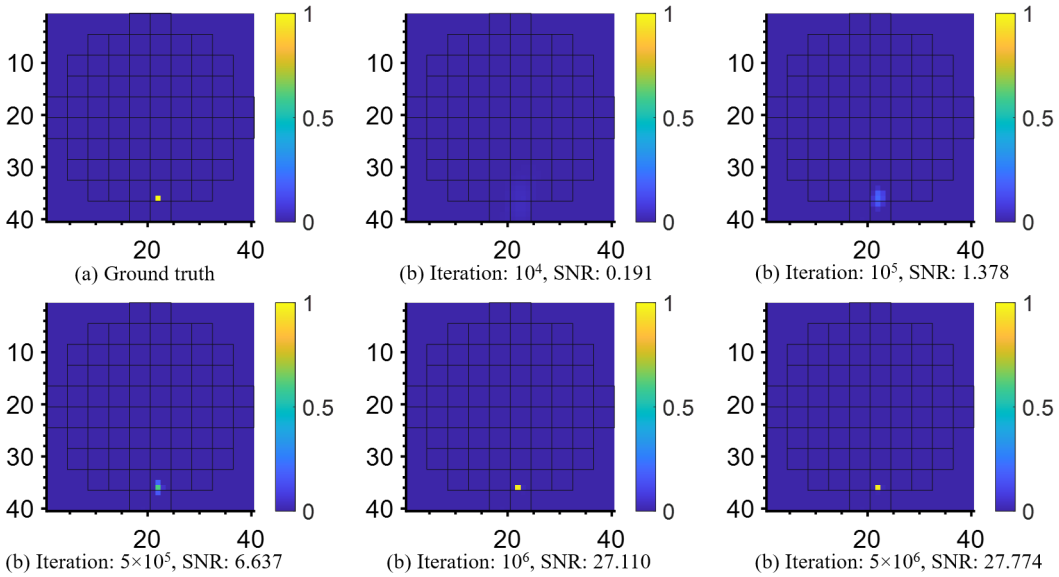

Figure 7: Reconstructed images from FISTA with different number of iterations.

6. Application of the CNN to the Reconstructed Images

Well reconstructed images for the peripheral assemblies can be obtained using the iterative FISTA algorithm as shown in Fig. 7. However, for the inner assembly missing scenarios, the quality of reconstructed images using FISTA is decreased. Fig. 8 shows the ground truth where inner pins ($\frac{1}{16}$ pins of one fuel assembly) are missing and the corresponding reconstructed images from FISTA with maximum number of iterations set to 10^6. This is because when there are inner pins missing, the back-scattered signal will suffer more from the shielding effect of the outer fuel assemblies. Thus, we applied the CNN model to improve the reconstructed image quality.

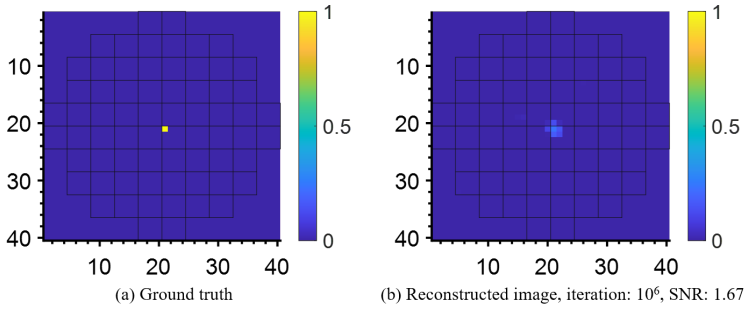

Figure 8: Ground truth and reconstructed image using FISTA algorithm for inner fuel pins missing scenario.

We first obtained the reconstructed images with different SNR ($\geq$ 2) for $\frac{1}{16}$ of fuel pins missing in one assembly across all fuel assembly locations. The reconstructed images were divided into two groups for the training (1200 images) and validation (400 images) purpose. In each group, we used high-quality images as the ground truth and low-quality images as the input to the network. The CNN results in Fig. 9 show that for the inner assemblies, the noisy input images reconstructed using the FISTA algorithm can be further improved by applying the trained CNN model.

7. Conclusion

In this study, we discussed the feasibility of using 14.1 MeV fast neutrons for tomographic imaging of a MPC-68 canister SNF canister. Based on the Monte-Carlo simulation study, we identified the back-scattered neutrons signature as the high-information-rich signature. The back-scattered neutrons showed a certain relationship with the location of the

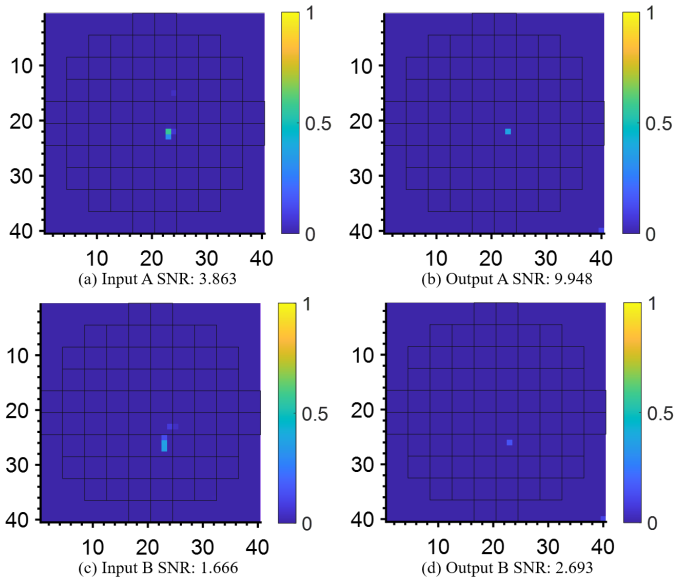

Figure 9: Reconstructed images from the CNN for the inner fuel region.

missing fuel assembly. We observed a drop of the back-scattered signal of 4.78% when one fuel assembly was missing at the shallowest location, i.e. the diversion scenario Case8. Then we applied an image reconstruction method to improve the correlation between the measured neutron signature and the location of the missing fuel assembly. The reconstructed images from FISTA algorithm show that the missing fuel assembly in the peripheral region can be accurately identified with maximum number of iterations set as 10^6. However, the reconstructed images quality are low for the mis-loaded inner fuel assemblies due to the increased noise. Thus, we combined the reconstructed images with the pre-trained CNN model, and the results show that the image quality can be further improved by CNN, such as shown in Fig. 9 the image quality was increased by 61% in the case of input B.

Acknowledgements

This work is funded in part by the Department of Energy (DOE) under contract number 000128931. The Argonne Leadership Computing Facility (ALCF) provided the access to super-computing resources.

References

[1] Transportation of spent nuclear fuel, https://www.nrc.gov/waste/spent-fuel-transp.html (jan 2020).

[2] D. S. Blair, A global perspective on continuity of knowledge: Concepts and challenges., Tech. rep., Sandia National Lab.(SNL-NM), Albuquerque, NM (United States) (2014).

[3] J. M. Durham, D. Poulson, J. Bacon, D. Chichester, E. Guardincerri, C. Morris, K. Plaud-Ramos, W. Schwendiman, J. Tolman, P. Winston, Verification of spent nuclear fuel in sealed dry storage casks via measurements of cosmic-ray muon scattering, Physical Review Applied 9 (4) (2018) 044013.

[4] D. Poulson, J. M. Durham, E. Guardincerri, C. Morris, J. D. Bacon, K. Plaud-Ramos, D. Morley, A. A. Hecht, Cosmic ray muon computed tomography of spent nuclear fuel in dry storage casks, Nuclear Instruments and Methods in Physics Research Section A: Accelerators, Spectrometers, Detectors and Associated Equipment 842 (2017) 48–53.

[5] S. Chatzidakis, Classification and imaging of spent nuclear fuel dry casks using cosmic ray muons, Oak Ridge, TN: Oak Ridge National Laboratory (ORNL).[Google Scholar] (2017).

[6] S. Agostinelli, J. Allison, K. a. Amako, J. Apostolakis, H. Araujo, P. Arce, M. Asai, D. Axen, S. Banerjee, G. . Barrand, et al., Geant4—a simulation toolkit, Nuclear instruments and methods in physics research section A: Accelerators, Spectrometers, Detectors and Associated Equipment 506 (3) (2003) 250–303.

[7] M. Fang, D. D. Latta, Y. Altmann, M. Salvatori, A. D. Fulvio, Comparison of Image Reconstruction Methods for Simulated Passive Gamma Emission Tomography, INMM 61st Annual Meeting, Baltimore, Maryland, USA, 2020.

[8] A. Beck, M. Teboulle, A fast iterative shrinkage-thresholding algorithm for linear inverse problems, SIAM journal on imaging sciences 2 (1) (2009) 183–202.

[9] K. Gong, J. Guan, K. Kim, X. Zhang, J. Yang, Y. Seo, G. El Fakhri, J. Qi, Q. Li, Iterative pet image reconstruction using convolutional neural network representation, IEEE transactions on medical imaging 38 (3) (2018) 675–685.

[10] R. Gonzalez, R. Woods, Digital image processing, 3rd edn upper saddle river (2008).